Modelization of surfactant flooding : Methodology for determining the interfacial tension function of surfactant concentration and salinity

Iryna Malinouskaya, Christophe Preux, Adeline Martin, Aline Delbos

Modelisation of surfactant flooding: Methodology for determining the interfacial tension function of surfactant concentration and salinity

I. Malinouskaya[a], C. Preux[a], A. Martin[a], A. Delbos[a]

[a]*IFP Energies Nouvelles, 1 et 4 avenue de Bois-Préau, 92852 Rueil-Malmaison Cedex - France*

Abstract

To predict accurately the amount of oil that can be recovered by a process of surfactant flood injection, a fine modelization of variation of interfacial tension between oil phase and aqueous phase with the reservoir conditions is required. Unfortunately, data of interfacial tension variation with all the parameters, *i.e.* temperature, salinity and surfactant concentration, are not always available when numerical simulation of the reservoir production is performed. In that case, interpolation is often used, but then can not be fully representative of the variations. The work presented here details a new numerical model used to describe interfacial tension with all the parameters listed below. This model fit well experimental data obtained for this study. The asymetry of the model allows to take into account the specificity of industrial formulations, when the interfacial tension at large salinities is different from interfacial tension at zero salinity. The protocol to determine experimental data of optimal salinity and interfacial tensions for such industrial formulations is detailled. The correlation described in this paper is also used to perform numerical experiments of injection of a formulation containing surfactant in porous media to recover oil. The 1D experiments are constructed using realistic parameters from litterature. Sensitivity to optimal salinity is described using the interfacial tension model developped here, as well as its impact on oil production.

Keywords: Surfactant flooding, Salinity, Interfacial tension, Simulation

1. Introduction

To increase oil recovery, the addition of surfactant to reduce interfacial tension is a method that has proven its efficiency [1, 2, 3, 4]. By reducing the interfacial tension between oil and brine, the sweep efficiency of the aqueous phase injection is strongly increased. To predict accurately the oil recovery that one can expect from field, studies involve the use of numerical simulation combined with experiments to feed the numerical model. During this step, the dynamic numerical model applied on the near pilot area will use the modified fluid properties according to the measurements obtained by the chemicals injected in the aqueous phase. When polymer is injected, viscosity is modified, for surfactant and alkali, interfacial tension between oil and brine changes. To be able to modify these parameters, specific tools are used such as PumaFlow [5] to model the dynamics of fluids in porous media in presence of EOR chemicals.

In the case of surfactant injection, the main parameter of the process is the interfacial tension between oil and water and its evolution with salinity, temperature and chemicals concentration. The values of interfacial tensions are not always easy to obtain and often variations with salinity and temperature are not measured. These data are needed as the aqueous phase, during its flow from well to deep reservoir, may encounter brines at different temperatures and different salinities. In this case, a numerical model of variation of the interfacial tension is required by the simulator to get an accurate estimation of the oil displacement at each step of the simulation.

Models to determine the interfacial tension are largely studied, for example, by [6], more recentely [7]. Some links between curvature and interfacial tension are also studied, for example, by [8] and between micro structure and measurement at macroscopic scale [9]. Unlike cases cited here, is addressed here the case of industrial surfactants. This implies to take into account specificities of solution of surfactants including process residue and distribution of organic chain for the surfactant. The model take into account the macroscopic effect of surfactant on the interface.

This paper details first the classical methodology used to measure interfacial tension during a chemical EOR feasibility study. Then, a new numerical model which is used to predict variation of interfacial tension between organic phase and aqueous phase in presence of surfactants selected to reach ultra-low interfacial tension, is detailed. Analytical model for IFT can be very useful in reservoir simulation: the derivation is easier and can be impor-

tant for scheme implicitation. Moreover, history matching and sensitivity analysis is easier with analytical modelisation than with tabulation. This numerical model can also compensate the lack of experimental data in real cases. The model is successfully confronted with experimental data obtained for a typical industrial formulation encountered in industry.

2. Protocol and methodology to determine interfacial tension

A generalized description of the water-oil interfacial tension (IFT) behavior in the presence of surfactants proposed in the present paper is based on experimental measurements. These measurements are used to obtain required for a proposed analytical model parameters for a given surfactant. The choice of the surfactant and brine used in the experiments are provided in this Section, as well as the description of the methodology which allows to obtain the IFT. Since the interfacial tension variations with the surfactant concentration are already well-studied, the experiments are focused on the effects of the brine salinity.

2.1. Parameters

Experiments were performed with dodecane as reference oil model. This oil is an alkane which is known to be representative of a variety of low viscosity light crude oils, *i.e.* it exhibits similar Equivalent Alkane Carbon Numbers (EACN) [10] and gives a microemulsion with the same salinities as the oil it represents.

In order to set the tests, a brine type *seawater* (presence of divalent ions) is chosen. Seawater, often used in offshore applications, has a salinity of approximately 35 g/L TDS with hardness R^+

$$R^+ = \frac{[Ca^{2+}] + [Mg^{2+}]}{\sum [\text{cations}]} = 0.13 \text{ at } 40°\text{C} \tag{1}$$

Surfactants used in a surfactant polymer or alkali surfactant polymer (SP/ASP) injection context are mainly anionic. Here is chosen a mixture of IOS (Internal Olefins Sulfonates) and AGES (Alkyl Glyceryl Ether Sulfonates). These both surfactants are stable for a wide range of temperatures [11, 12].

To evaluate all the possibilities, tests were performed at different temperatures. For each temperature, salinity scans were carried out in order to

Formulation	IOS 4g/L + AGES 4g/L
Oil	Dodecane (C12)
Brine (present salts)	$NaCl$; KCl; $CaCl_2$ $2H_2O$; $MgCl_2$ $6H_20$

Table 1: Characteristics of the fluids used for our experiments.

determine the optimal salinity s^*. From this information, interfacial tension (IFT) values were measured and/or calculated.

The experiment conditions are summarized in Table 1.

2.2. Salinity scan and optimal salinity

The optimal salinity is the salinity at which the aqueous solution allows the surfactant to be as poorly soluble in the aqueous solution as in the oil. Consequently, all surfactants are found at the interface between these two phases. To determine this optimal salinity, different authors [13, 6] carried out a salinity diagram by bringing the oil into contact with different aqueous phases of constant surfactant concentration and increasing salinities. The appearance in the tubes of an intermediate phase between the oil and the aqueous phase indicates the salinities for which the interfacial tension is ultra-low. This situation is referred to as the Winsor III system.

In our experience, Baseline formulation has been prepared in brines seawater of increasing salinities, in regular steps, at each temperature (Figure 1). Each system clearly exhibits a Winsor I to Winsor III transition with an ultra-low interfacial tension region corresponding to the optimal salinity s^*. The ranges are placed in thermostatically controlled ovens and kept for 21 days.

2.3. Interfacial tension measurements

The interfacial tension at Winsor III is then determined using an experimental measurement method with the spinning drop tensiometer. This technics allows to obtain a water-oil IFT, contrary to, for example, Huh law, which yields an IFT between microemulsion and water, and IFT between microemulsion and oil.

A drop of light phase, here dodecane, of density ρ_l measured for each temperature tested, is injected into a glass capillary tube filled with heavy phase, baseline formulation, of density ρ_h also measured for each temperature tested. This tube undergoes rotation causing an elongation of the drop along

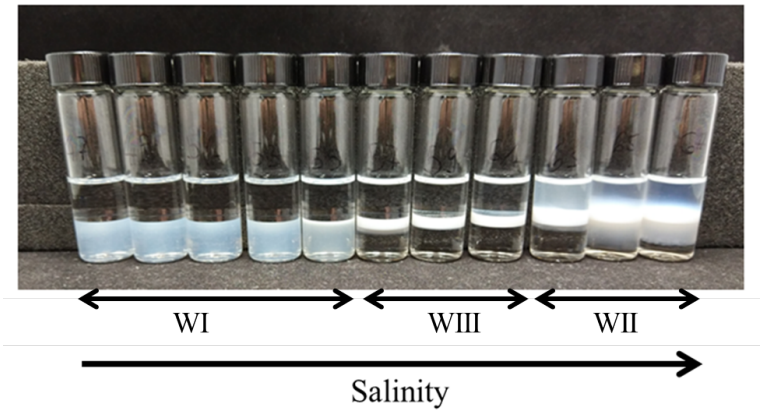

Figure 1: Salinity scan. Tubes are filled with 50% oil and 50% aqueous phase. When surfactant is in the aqueous phase the system is at Winsor I (WI). When surfactant is in the organic phase, system is at Winsor II (WII). When surfactant is concentrated at the interface system is at Winsor III (WIII).

the axis of rotation (Figure 2). IFT is measured from the radius of the curvature of the droplet.

According to Vonnegut's relation, and provided that the drop is at least four times longer than high, the IFT depends on the radius of the drop r, the angular speed ω and the difference in densities of heavy phase ρ_h and light phase ρ_l

$$IFT = \frac{r^3\omega^2(\rho_h - \rho_l)}{4} \tag{2}$$

2.4. Experiments settings

The experiments shown here are conducted for temperatures 20 et 40°C. After having carried out all the salinity scans as well as determining the optimal salinity at each temperature, the interfacial tensions are measured. In order to study the IFT behavior with respect to salinity variations, the measurements where performed for 5 different values:

- optimal salinity s^*, $IFT_{opt} = IFT(s^*)$;
- 2 values close to optimal salinities;
- 2 limit salinities, $IFT_{max} = IFT(s \to 0)$ and $IFT_{min} = IFT(s \to \infty)$.

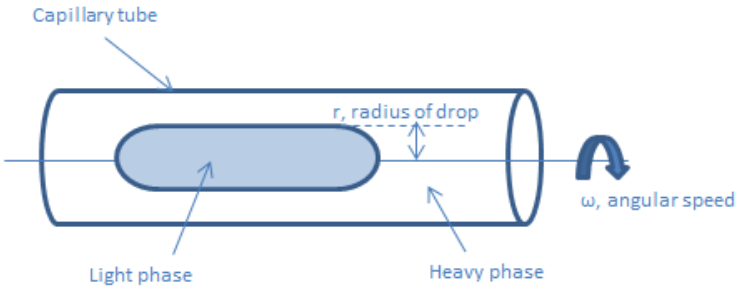

Figure 2: Sketch of the spinning drop device.

Measurements with spinning drop are reproduced 3 times. Values of interfacial tension are taken at the equilibrium.

3. Experiments Results

The results of the experiments set previously are provided in this Section. We are interested in the IFT behavior with the brine salinity variations. The results of the optimal salinity measurements are presented first. Then, the results of the interfacial tension for the key values of the salinity, as given in the experiment settings (Section 2.4), are provided.

3.1. Optimal salinity s^*

For each temperature, after an initial salinity scan, the system clearly exhibits a Winsor I to Winsor III transition with an ultra-low interfacial tension region (Figure 3). A second, finer salinity scan between the two identified target values was therefore carried out (Figure 4). This results were obtained after 21 days of equilibrium at given temperature T.

Table 2 summarizes results for each T.

3.2. Interfacial tension

Taking into account the salinity scan results, the IFT is measured for $s = s^* = 69$ g/L, for $s = 67$ and 71 g/L, as well as at the far limits $s = 0$ and 100 g/L, for the temperature of 20°C. Similarly for 40°C, the explored salinities are 0, 45, 49, 53 and 100 g/L. The resulting IFT are shown in Figure 5.

Figure 3: Large salinity scan at 40°C.

Figure 4: Finer salinity scan at 40°C.

Temperature, [°C]	20	40
Salinity range of ultra-low IFT, [g/L]	65-75	44-54
Optimal salinity s^*, [g/L]	69	49

Table 2: Ultra-low interfacial tension salinity region and optimal salinity for each temperature.

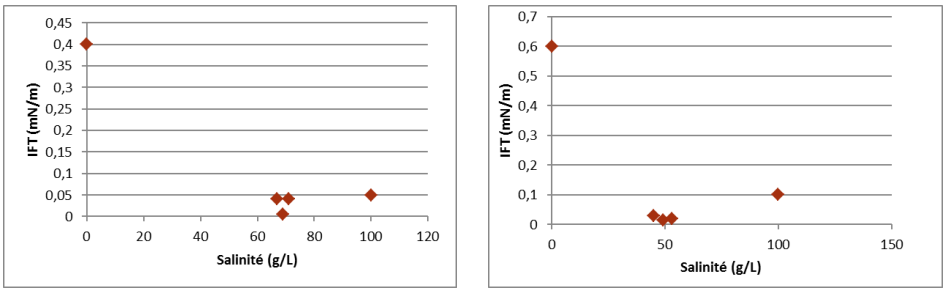

(a) (b)

Figure 5: IFT measurements with spinning drop tensiometer versus salinity at 20°C (a) and 40°C (b).

Thus, at the optimal salinity, IFT_{opt} is found 0.005 mN/m for 20°C and 0.015 mN/m for 40°C. At the limiting salinities, one get $IFT_{max} = 0.4$ mN/m for 20°C and 0.6 mN/m for 40°C, and $IFT_{min} = 0.05$ and 0.1 mN/m for 20 and 40°C, respectively.

These results are required to get a full description of the IFT behavior versus salinity, as provided below.

4. Correlation determination

This Section addresses an analytical formulation proposed to obtain the generalized curve of the water-oil interfacial tension for any surfactant concentration/salinity combination using the experimental results (Section 3).

4.1. The dependence of IFT on salinity

In [14], the authors propose a correlation of IFT with salinity. This correlation is based on the assumption that $IFT_{max} = IFT_{min}$. However, there is a number of surfactant for which it is not true as, for example, the baseline formulation which is used here. Therefore, based on the correlation of [14], a slightly different formulation is proposed [15]

$$IFT(s) = IFT_{opt} \left(\frac{F(s)}{IFT_{opt}} \right)^{1-\exp\left(-\frac{(s-s^*)^2}{w(s)^2}\right)} \tag{3}$$

where $F(s)$ is a function which yields $F(s \to 0) = IFT_{max}$ and $F(s \to \infty) = IFT_{min}$, and the function $w(s)$ is the salinity window.

In the present work, the following expression for $F(s)$ is proposed

$$F(s) = \frac{1}{2}\left(IFT_{max} + IFT_{min}\right) - \frac{1}{\pi}\tan^{-1}\left(\frac{s-s^*}{\delta}\right)\left(IFT_{max} - IFT_{min}\right) \tag{4}$$

where parameter δ is chosen according to a targeted smoothness of the switchover from IFT_{max} to IFT_{min}. For a while, δ is set to 0.01. This value means that $F(s^* + 1g/L) = IFT_{min}$ and $F(s^* - 1g/L) = IFT_{max}$ within 1%.

Consider the salinity window $w(s)$ with respect to the optimal salinity s^* as a linear function of s which is written as

$$w(s)s^{*-1} = a + bs \tag{5}$$

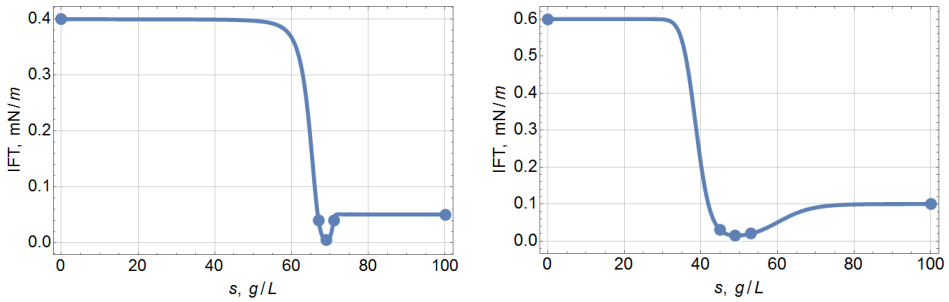

(a) (b)

Figure 6: IFT correlation as function of salinity for 20°C (a) and 40°C (b).

Temperature, [°C]	a, [ ]	b, [L/g]
20	-0.32036	0.004242
40	0.05152	0.002831

Table 3: Fitted values of parameters a and b for the IFT curves.

The IFT correlation is, then, obtained by regression on a and b using at least two measurements close to the optimal salinity.

The parameters IFT_{opt}, IFT_0, IFT_{min} , IFT_{max} and CMC are macroscopic parameters. Only a and b used to fit the salinity window are the parameters linked to the surfactant interaction with salts, *i.e.* to the polar part of the surfactant. A sulphonated surfactant which is the most common surfactant used for EOR application is used here. The a and b values can be considered for all those kind of surfactants. Since the purpose of the study is to demonstrate the application of our IFT model, only one kind of surfactant is used as an example. However, for other kinds of surfactants, the model parameters a and b can be deduced in the similar way according to the measured macroscopic parameters (IFT_{opt}, IFT_0, IFT_{min} , IFT_{max} and CMC) in order to obtain the corresponding IFT model given by (3-5).

Thus, using the measurements shown on Figure 5, the IFT curves are obtained as functions of salinity for each temperature, 20 or 40°C (Figure 6), with the parameters a and b given in Table 3.

The found values of a and b yield very small variations of salinity window $w(s)$ within the ultra-low IFT salinity range for both temperatures (Table 2). For the optimal salinity, $w(s^*)$ at 20°C is found of about 1.9 g/L while

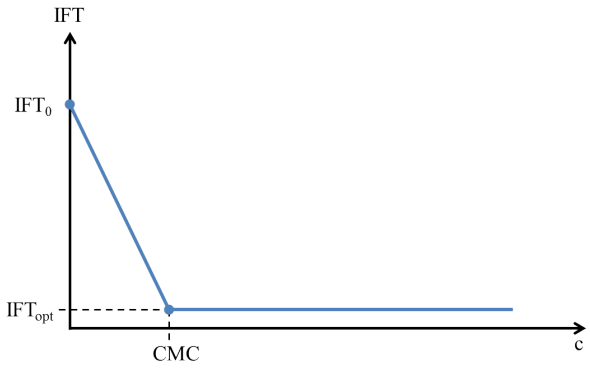

Figure 7: Schematic IFT behavior with the surfactant concentration.

for 40°C it is about 9.3 g/L.

4.2. The dependence of IFT on surfactant concentration

Through experimental studies, it is well-known that the water-oil interfacial tension behavior is very sensitive to the surfactant content until it reaches its critical micelle concentration (CMC) as schematically shown in Figure 7. Thus, for the surfactant injection simulations, the IFT variations with the surfactant concentration should imperatively be taken into account.

In the software Pumaflow^{TM}, the following correlation is proposed

$$IFT(c) = IFT_\infty \left(\frac{IFT_0}{IFT_\infty} \right)^{\exp\left(-\frac{c}{CMC} \ln\left(\frac{IFT_0}{IFT_\infty}\right)\right)} \tag{6}$$

where c is the concentration of surfactant, CMC is the critical micelle concentration, $IFT_0 = IFT(c = 0 \text{ g/L})$ and $IFT_\infty = IFT(c \to \infty)$.

It should be noted, that IFT_0 as well as IFT_∞ are salinity and temperature dependent. However, for the experiments represented here, IFT_0 does not vary a lot in the considered temperature and salinity ranges, therefore, let us consider it as a constant. On the other hand, IFT_∞ salinity dependence can be expressed by $IFT(s)$ obtained by (3).

The temperature effects are not studied here. The measurements for 20 et 40°C are only used in order to get the corresponding fitted curves of $IFT(s)$.

4.3. Summary of IFT correlation

Using the IFT surfactant concentration and the salinity dependences (6) and (3), a general correlation $IFT(c,s)$ is obtained in the following form

$$IFT(c,s) = IFT(s)\left(\frac{IFT_0}{IFT(s)}\right)^{\exp\left(-\frac{c}{CMC}\ln\left(\frac{IFT_0}{IFT(s)}\right)\right)} \tag{7}$$

with

$$\begin{aligned} IFT(s) &= IFT_{opt}\left(\frac{F(s)}{IFT_{opt}}\right)^{1-\exp\left(-\frac{(s-s^*)^2}{(a+bs)^2 s^{*2}}\right)}, \\ F(s) &= \tfrac{1}{2}\left(IFT_{max}+IFT_{min}\right) - \tfrac{1}{\pi}\tan^{-1}\left(\tfrac{s-s^*}{\delta}\right)\left(IFT_{max}-IFT_{min}\right) \end{aligned} \tag{8}$$

Thus, using a limited number of the surfactant measurements, the general formulation allows to get a good description of the IFT evolution during the numerical simulations of the surfactant injection under various salinity/concentration conditions.

5. Numerical experiments

This section addresses the application of the previously obtained IFT correlations and study the sensitivity of this method using Pumaflow^{TM} software based on a fully implicit scheme [17, 18]. In this purpose, a simple 1D model is constructed based on the realistic parameters detailed in [16].

5.1. Core sample

A Berea Sandstone core is considered with the relevant properties given by [19, 20, 21] and listed in Table 4.

5.2. Reservoir specification

The core sample pressure is set to 1 bar. The oil viscosity is constant equal to 1 cP. Since the thermal effects are not a subject of the present study, let us set the reservoir at constant temperature, $T = 20°\mathrm{C}$.

Diameter [cm], [19]	5.08
Length [cm], [19]	30.48
Porosity [-], [20]	0.22
Permeability [mD], [19]	776
Compressibility [bar$^-$1], [21]	0.25×10^{-5}
Irreducible water saturation S_{wi} [-], [20]	0.35
Residual oil saturation S_{or} [-], [20]	0.36

Table 4: Core properties.

5.3. Brine

A reservoir brine corresponds to one used for the previous experiments (Table 1). In the numerical model, it is represented through one pseudo ion of the molar mass 31.6 g/mol and initial concentration 35 g/L which corresponds to the reservoir brine salinity.

As shown by measurements (Section 3) for the temperature $T = 20°$C, the optimal salinity of 69 g/L was obtained for the surfactant concentration of 8 g/L. However, taking into account the IFT behavior as function of c (Figure 7) given by equation (6), far from CMC, the IFT does not vary with the surfactant concentration. Therefore, in the numerical simulations it is chosen to inject 3 g/L of the surfactant within the brine with the ion concentration of 69 g/L.

The brine viscosity is constant and equals to 1 cP.

5.4. Surfactant model and water-oil interfacial tension

The baseline formulation, the mixture of surfactants used for the IFT measurements (Table 1), is implemented for the numerical experiments. There is no surfactant adsorption considered in the present study.

Then, using the experimental measurements obtained at 20°C, the water-oil interfacial tension can be obtained by the formulation (7, 8) with the parameters given in Table 5.

In Figure 8a, the resulting curves of IFT as a function of the surfactant concentration c is shown for the optimal salinity $s = s^* = 69$ g/L, for the salinities closed to s^*, *i.e.*, $s = 67$ and 71 g/L, and for the limits $s = 0$ and 100 g/L. Then, in Figure 8b, the resulting IFT is plotted as a function of the salinity s for three values of c, $c =$ CMC/2, $c =$ CMC and $c = 3$ g/L which corresponds to the concentration of the surfactant in the injection brine.

s^*, [g/L]	69
CMC, [g/L]	0.1
IFT_{opt}, [mN/m]	0.005
IFT_0, [mN/m]	30
IFT_{max}, [mN/m]	0.4
IFT_{min}, [mN/m]	0.05
a, [-]	-0.32036
b, [L/g]	0.004242

Table 5: The parameters used for the $IFT(c, s)$ (7, 8).

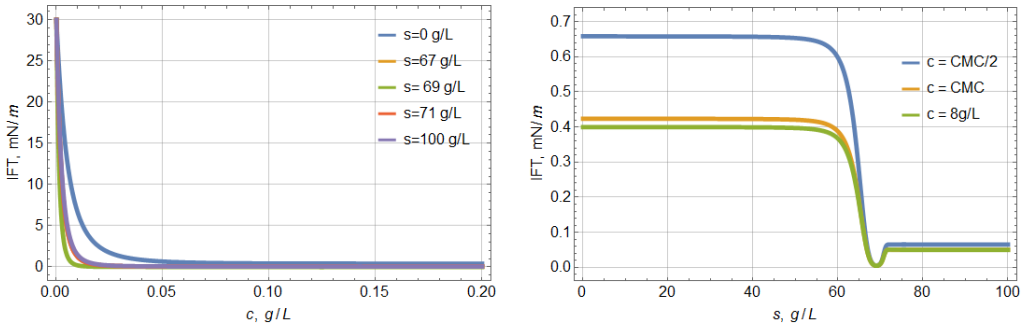

(a) (b)

Figure 8: IFT as function of surfactant concentration for a few salinity values (a) and as function of salinity for a few fixed values of the surfactant concentration within the "transition" range and far from CMC.

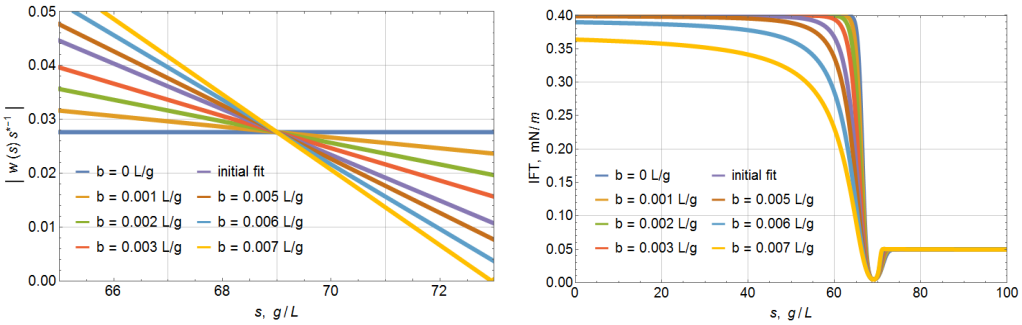

(a) (b)

Figure 9: (a) Studied variations of the salinity window $w(s)s^{*-1}$ (9) and (b) the corresponding IFT (7, 8) calculated for the surfactant concentration $c = 3$ g/L.

In the proposed IFT model (7, 8), the parameters a and b are obtained through the results of the IFT measurements within the ultra-low IFT salinity range. We would like to demonstrate the sensitivity of the proposed IFT formulation to the quality of these measurements and precision of the fitted values a and b.

Let us remind here that the parameters a and b are directly related to the salinity window $w(s)$ (5). Suppose that at the optimal salinity, $w(s^*)s^{*-1}$ is correctly identified by (5). Then, the uncertainty element is the slope which characterize how fast the salinity window changes around the optimal salinity range. Thus, one obtains

$$w(s)s^{*-1} = w(s^*)s^{*-1} + b(s - s^*) \tag{9}$$

Therefore, for the sensitivity analysis, the formulation (9) is used with the variation of slope b in the range $b \in [0, 0.007]$ L/g.

The studied variations of the salinity window $w(s)s^{*-1}$ and corresponding to them IFT are shown in Figure 9. The formulation (9) yields that at the optimal salinity, the interfaciel tension equals to IFT_{opt} for any b. For $b \leq 0.005$ L/g, the IFT at the extreme values of salinity ($s = 0$ and 100 g/L) differ from the measured values by less than 1%, while for $b = 0.006$ and 0.007 at zero salinity, IFT is obtained, respectively, 3 and 9% smaller than IFT_{max}.

Thus, the major influence of the measurements/fit precision will be captured in the range of salinity which corresponds to the transition between IFT_{max} and IFT_{opt}; roughly, it is within $s \in [50, 65]$ g/L.

Parameters	Low N_c	High N_c
S_{wi}, [-]	0.35	0
S_{or}, [-]	0.36	0
Kr_w^{max}, [-]	0.4	1
Kr_o^{max}, [-]	0.95	1
n_o, [-]	2	1
n_w, [-]	5	1

Table 6: End-points of relative permeability curves for lowest and highest capillary number N_c.

5.5. Relative permeability and capillary desaturation curve (CDC)

Consider a water-wet core sample. The water-oil interfacial tension impacts the surfactant flooding by means of capillary number N_c which characterizes the ratio between viscous and capillary forces

$$N_c = \frac{\mu_w \|\overrightarrow{u_w}\|}{IFT} \tag{10}$$

where μ_w is the water viscosity and $\|\overrightarrow{u_w}\|$ is the norm of the water phase velocity.

Then, the relative water and oil permeabilities, Kr_w and Kr_o, respectively, depend on N_c and can be obtained by an analytical model. Based on Corey formulation [22] and according to the rules of the thumb [24, 25], detailed in [23], the relative permeability curve is defined for a low capillary number. Considering a totally miscible flow for a high capillary number, the Corey end-point are trivial. These two sets of relative permeability end-points are provided in Table 6 and the relative water and oil permeabilities are obtained by

$$\begin{aligned} Kr_w(S_w, N_c) &= Kr_w^{max}(N_c) \left(\frac{S_w - S_{wi}(N_c)}{1 - S_{wi}(N_c) - S_{or}(N_c)} \right)^{n_w(N_c)} \\ Kr_o(S_o, N_c) &= Kr_o^{max}(N_c) \left(\frac{S_o - S_{or}(N_c)}{1 - S_{wi}(N_c) - S_{or}(N_c)} \right)^{n_o(N_c)} \end{aligned} \tag{11}$$

where n_w and n_o are the Corey parameters for water and oil phases, respectively, S_{wi} the irreducible water saturation, S_{or} the residual oil saturation, Kr_w^{max} and Kr_o^{max} the end-points for the relative permeabilities, S_w and S_o the water and oil saturations.

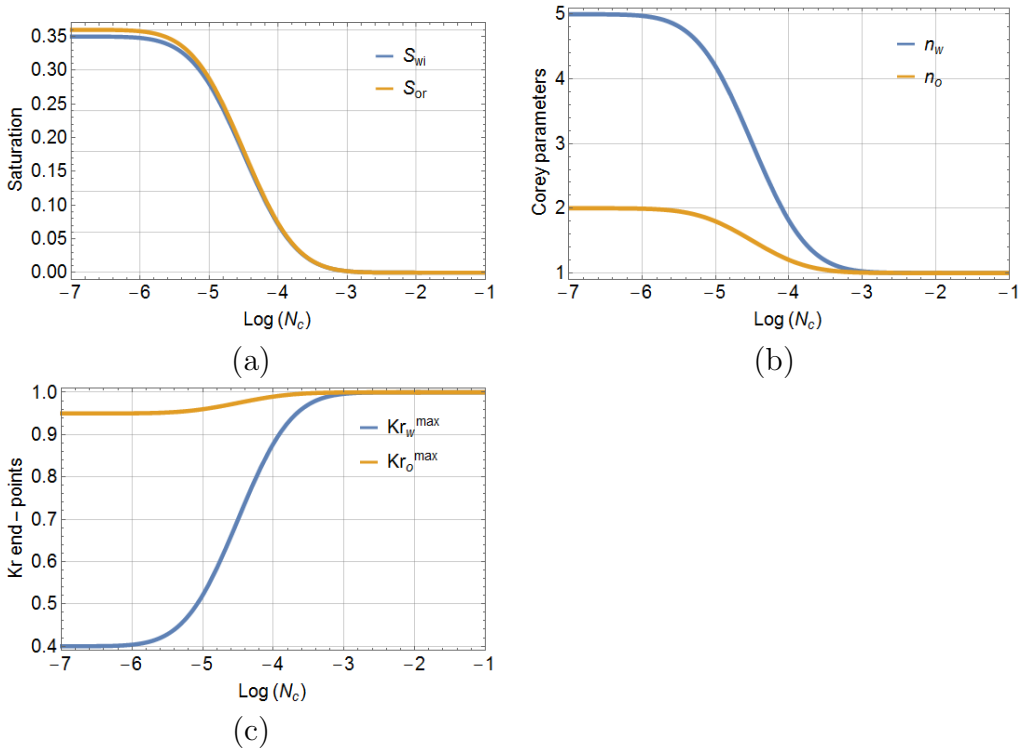

Figure 10: The end-points (Table 6) dependence on the capillary number N_c given in [26, 27].

The capillary desaturation curve (CDC) describe the decrease of the residual oil saturation with respect to the capillary number N_c, and it can be obtained by an analytical formulation proposed by [26]. Consequently, the irreducible water saturation and the Corey parameters, can be obtained in the same form [27]. The end-points of the relative water and oil permeabilities are then obtained as given in [26]. The corresponding curves are shown in Figure 10.

6. Results and discussion

Initially, the core is water saturated with $S_w = 1 - S_{or} = 0.64$. The brine with surfactant is injected at constant rate of 0.001 m^3/day during about 0.04 days, then, the brine without surfactant continue to be injected till 0.6

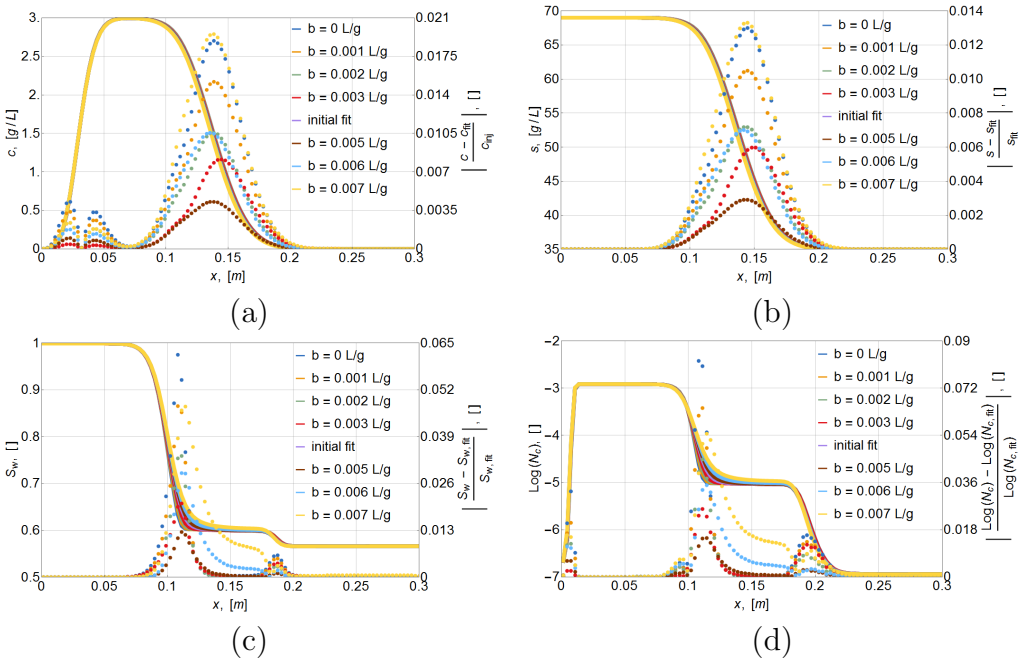

Figure 11: The resulting surfactant concentration (a), salinity (b), water saturation (c) and capillary number (d) in the core at time ≈ 0.054 days ≈ 4 injected pore volumes (IPV) . The dots (right-hand axis labels) correspond to the relative difference between the results for various b and those obtained using its fitted value.

days. The production well is controlled through a constant pressure equal to 1 bar.

6.1. IFT correlation sensitivity

The modification of the window around the optimal salinity does not affect the optimal salinity but only the shape.

As described in Section 5.4, the sensitivity of the results to the precision of the IFT model is studied first. For this, the numerical simulations are performed with the interfacial tensions obtained as shown in Figure 9b for various slopes b of the salinity window (9). Brine is injected at the optimal salinity.

In Figure 11, the results for the surfactant concentration c, the salinity s, the water saturation S_w and the logarithm of the capillary number $\log(N_c)$ are shown within the core at time 0.054 days, which corresponds to approximately 4 injected pore volumes. The impact of the studied IFT models is

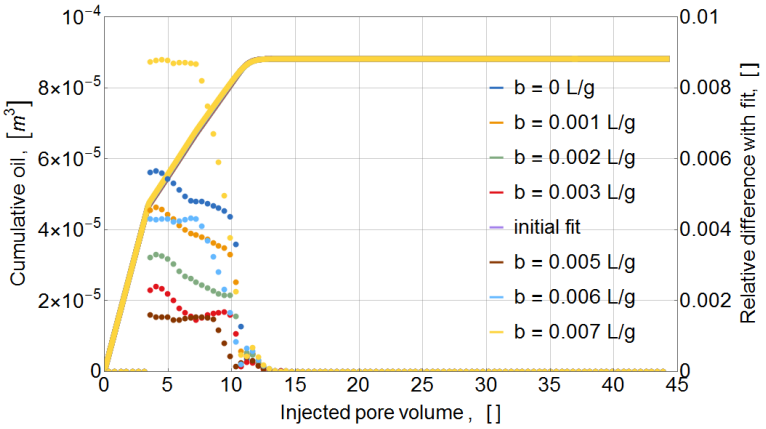

Figure 12: The produced oil for various slopes b of the salinity window. The dots (right-hand axis labels) correspond to the relative difference between the results for various b and those obtained using its fitted value.

insignificant and do not exceeds 10% compared to the results obtained with the initial fit given by parameters in Table 5. The surfactant concentration and the salinity are definitely unaffected by the IFT variations, while the major differences in the capillary number and water saturation are obtained in a transition ranges between maximum and minimum values of c and s.

Since, at the optimal salinity, the IFT is the same for all the cases, then only transitory profiles are modified. Thus, in Figure 12, the oil production differences are observed while the core salinity doesn't achieve the value of the optimal salinity. Finally, the same volume of oil is produced for all the cases.

6.2. Optimal salinity sensitivity

In order to demonstrate the error in the oil production estimation induced by a slightly inaccurate measurements of the optimal salinity, four simulations are performed.

Suppose that the interfacial tension given by (7, 8) with parameters from Table 5, is exact for a given surfactant. Then, consider the salinity of the injected fluid is $\pm 1\%$ and $\pm 3\%$ wrong compared to $s^* = 69$ g/L, *i.e.*, $s_{inj} =$ 66.93, 68.31, 69.69 and 71.07 g/L. In Figure 13, these points are shown on the used IFT curve. The interfacial tension for the salinities $s^* \pm 1\%$ is 42 and 56 % higher than expected IFT_{opt} and for $s^* \pm 3\%$ it is about eight times

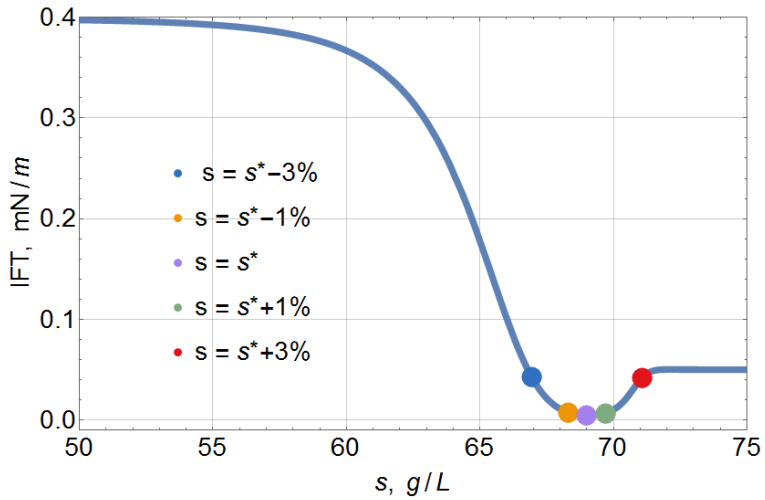

Figure 13: IFT points corresponding to studied errors on the optimal salinity.

higher.

The results within the core at 4 injected pore volumes are shown in Figure 14. For the surfactant concentration and the salinity, the major differences are observed on transitory profiles which is related to the mobility reduction due to the interfacial tensions. For the injected salinity $s_{inj} < s^*$, the IFT have never reached IFT_{opt} and, consequently, the profiles are in advance compared to the case of $s_{inj} = s^*$. Similarly, for $s_{inj} > s^*$, the profiles are delayed according to the difference in IFT, but the relative error is insignificant and does not exceeds 4% for c and 2% for s. Obviously, on backward of the injection front, the salinity is established to the corresponding s_{inj} values.

The analysis of the water saturation and the capillary number profiles is more complicated (Figure 14c, d). They are influenced not only by the interfacial tensions, but also by the capillary desaturation (Figure 10). However, the cases with $s_{inj} = s^* \pm 1\%$ are closed to the results with true optimal salinity, while the cases of $s_{inj} = s^* \pm 3\%$ yield more significant differences due to the corresponding IFT for current (c, s) values.

In Figure 15, the error in the oil production estimation induced by the optimal salinity is demonstrated. When using $s_{inj} = s^* \pm 1\%$, there is no significant impact on the production results. Then, for $s_{inj} = s^* + 3\%$, the produced oil is slightly underestimated by about 2.5% while for $s_{inj} = s^* - 3\%$ the difference is about 8%. Injecting the salinity superior of s^*, the core

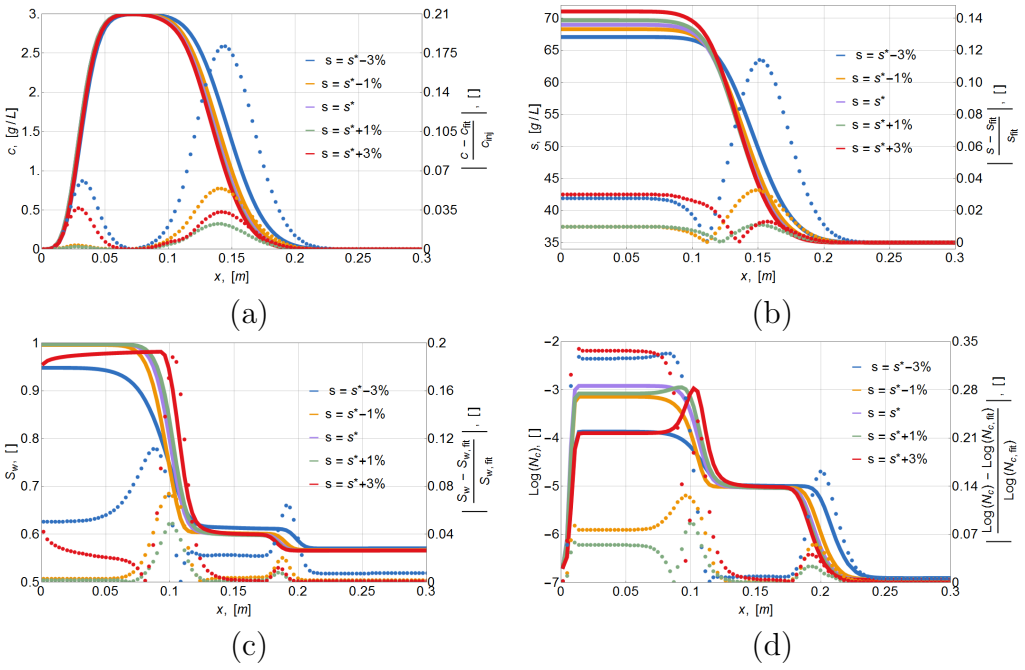

Figure 14: The surfactant concentration (a), salinity (b), water saturation (c) and capillary number (d) in the core at ≈ 4 IPV) . The dots (right-hand axis labels) correspond to the relative difference between the results for various s_{inj} and those obtained for $s_{inj} = s^*$.

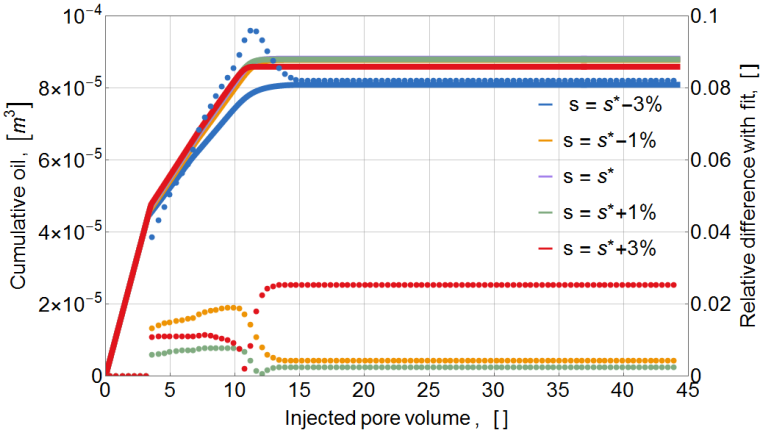

Figure 15: The produced oil for various errors in optimal salinity s^*. The dots (right-hand axis labels) correspond to the relative difference between the results for various s_{inj} and those obtained for $s_{inj} = s^*$.

salinity will reach first the value $s = s^*$, for which the interfacial tension is optimal, and it allows the better oil sweep before the salinity reaches s_{inj}. On the contrary, when $s_{inj} < s^*$, the IFT keeps always higher than IFT_{opt}, and, therefore, the oil production estimation is worse than for the case of $s_{inj} > s^*$.

Thus, for the oil production estimation using the proposed interfacial tension model (7, 8), the determination of the optimal salinity reveals more important than the variation of the salinity window around this value.

7. Conclusions

In this paper, the model of the interfacial tension which vary with the surfactant and salt concentration for realistic industrial surfactants is determined. It allows to predict the interfacial tension with a good accuracy compared to the experimental data. This model can then be used to perform numerical simulations of the surfactant injection in a porous media in order to estimate its behavior in realistic conditions.

The sensitivity of the proposed IFT model to the various included parameters was studied. This example reveals a possible errors in the oil production estimation due to the errors in the IFT model parameters.

The study conducted here allows to get a full modelization of flooding experiment including a realistic variation of interfacial tension with the different parameters involved with a minimum of data from laboratory experiments which are often missing during the first steps of faisability study for the surfactant injection in reservoir.

Main results of this paper are a new model which allows to capture the salinity and surfactant concentration variation in the interfacial tension behavior based on a few laboratory measurements, and the application of this model for the oil production estimation through the numerical simulations under different reservoir/injection conditions.

It should be noted, that in the present study, the surfactant injection was studied for a constant temperature. However, for the important differences between surface and reservoir temperatures, the IFT behavior with the temperature should be included in the model at the next step of the study.

To go further, new chemistries or new combination of surfactants could be evaluated using the proposed model.

Acknowledgements

Authors thanks Aurelie Mouret and Corinne Burnichon for fruitful discussions and Calista Kahn for experiments she conducted during her internship.

[1] Reppert, T. R., Bragg, J.R., Wilkinson, J.R., Snow, T.M., Maer, N.K., Gale, W.W., (1990). Second Ripley Surfactant Flood Pilot Test. SPE/DOE Enhanced Oil Recovery Symposium, 22-25 April, Tulsa, Oklahoma. DOI: https://doi.org/10.2118/20219-MS

[2] Bragg, J. R., Gale, W.W., McElhannon, W.A., Davenport,Jr, O. W., Petrichuck, M. D., Aschcraft, T.L. (1982). Loudon Surfactant Flood Pilot Test. SPE Enhanced Oil Recovery Symposium, 4-7 April, Tulsa, Oklahoma. DOI: https://doi.org/10.2118/10862-MS

[3] Volokitin, Y., Shuster, M., Karpan, V., Kolsov, I., Mikhaylenko, E., Bondar, M., Podberzhny, M., Rakitin, A., Van Batenburg, D.W., Parker, A. R., De Kruijf, S., Southwick, J. G., De Reus, J., Van Den Pol, E., Van Der Heyden, F.H.J., Boels, L., Wever D.A.Z., Brewer, M. (2018). Results of alkaline surfactant polymer flooding pilot at West Salym Field. SPE EOR Conference at Oil and Gas West Asia, 26-28 March, Muscat, Oman. DOI: https://doi.org/10.2118/190382-MS

[4] Puskas, S., Vago, A., Toro, M., Ordog, T., Kalman, G., Hanzelik, P., Bihari, Zs., Blaho, J., Tabajdi, R., Dekani, I., Dudas, J., Nagy, R., Bartha, L., Lakatos, I. (2018). Surfactant-polymer EOR from laboratory to the pilot. SPE EOR Conference at Oil and Gas West Asia, 26-28 March, Muscat, Oman. DOI: https://doi.org/10.2118/190369-MS

[5] Al-Murayri, M.T., Abdulgadir Hassan, A., Al-Mahmeed, N., Suzanne, G., Sanchez, J. P. (2018). Surfactant Polymer flooding: one spot EOR pilot design for a middle eastern heavy oil reservoir. SPE International Heavy Oil Conference and Exhibition, 10-12 December, Kuwait City, Kuwait. DOI: https://doi.org/10.2118/193743-MS

[6] Huh, C. (1979). Interfacial tensions and solubilizing ability of a microemulsion phase that coexists with oil and brine. Journal of Colloid and Interface Science, 71(2), pp 408-426. DOI: https://doi.org/10.1016/0021-9797(79)90249-2

[7] Sottmann, T. and Strey, R. (1997). Ultralow interfacial tensions in water-n-alkane-surfactant systems. J. Chem. Phys., 106, 8606. DOI:https://doi.org/10.1063/1.473916

[8] Strey, R. (1994). Microemulsion microstructure and interfacial curvature. Colloid Polym Sci 272, pp 10051019. https://doi.org/10.1007/BF00658900

[9] Fukumoto, A., Dalmazzone, C., Frot, D., Barré, L. and Noïk, C. (2016). Investigation on Physical Properties and Morphologies of Microemulsions formed with Sodium Dodecyl Benzenesulfonate, Isobutanol, Brine, and Decane, Using Several Experimental Techniques. Energy & Fuels, 30 (6), pp 4690-4698. DOI: https://doi.org/10.1021/acs.energyfuels.6b00595

[10] Salager, J., Forgiarini, A.M., Márquez, L., Manchego, L., Bullón, J. (2013). How to Attain an Ultralow Interfacial Tension and a Three-Phase Behavior with a Surfactant Formulation for Enhanced Oil Recovery: A Review. Part 2. Performance Improvement Trends from Winsors Premise to Currently Proposed Inter- and Intra-Molecular Mixtures. J Surfact Deterg 16, 631663. DOI: https://doi.org/10.1007/s11743-013-1485-x

[11] Tabary, R., Bazin, B., Douarche, F., Moreau, P., Oukhemanou-Destremaut, F. (2013). Surfactant Flooding in Challenging Conditions: Towards Hard Brines and High Temperatures. Society of Petroleum Engineers. DOI: https://doi.org/10.2118/164359-MS

[12] Delbos, A., Tabary, R., Chevalier, E., Moreau, P. (2014). Surfactant-Polymer Flooding in Hard Brines and High Temperature Reservoirs. International Petroleum Technology Conference, 10-12 December, Kuala Lumpur, Malaysia. DOI: https://doi.org/10.2523/IPTC-18208-MS

[13] Winsor P. (1954). Solvent properties of amphiphilic compounds. Butterworth Londres.

[14] Leray, S., Douarche, F., Tabary, R., Peysson, Y., Moreau, P., Preux, C. (2016). Multi-objective assisted inversion of chemical EOR corefloods for improving the predictive capacity of numerical models. Journal of Petroleum Science and Engineering, 146, pp 1101-1115. DOI: https://doi.org/10.1016/j.petrol.2016.08.015

[15] Malinouskaya, I., Preux, C., Martin, A., Delbos, A. (2020). Patent pending - application number FR 2020/05.675

[16] Preux, C., Malinouskaya, I., Nguyen, Q.L., Flauraud, E., Ayache, S.V. (2020). Reservoir simulation model with surfactant flooding including salinity and thermal effect, using laboratory experiments. SPE Journal. DOI: https://doi.org/10.2118/196663-PA

[17] Braconnier, B., Flauraud, E. and Nguyen, Q.L. (2014). Efficient Scheme for Chemical Flooding Simulation. Oil & Gas Science and Technology Rev. IFP Energies nouvelles, 69(4), pp. 585-601. DOI: https://doi.org/10.2516/ogst/2013189

[18] Braconnier, B., Preux, C., Flauraud, E., Tran, Q.H. and Berthon, C. (2017). An analysis of physical models and numerical schemes for polymer flooding simulations. Comput Geosci, 21, pp. 1267-1279. DOI: https://doi.org/10.1007/s10596-017-9637-0

[19] Ziegler, V. M. (1988). Laboratory Investigation of High Temperature Surfactant Flooding. SPE Reservoir Engineering, 3(2). DOI: https://doi.org/10.2118/13071-PA

[20] Moradi, H., (2011). Experimental Investigation of Polymer Flow Through Water- and Oil-wet Porous Media. Master's thesis in Petroleum engineering, University of Stavanger, Norway.

[21] Zimmerman, R. W. (1991). Compressibility of sandstones. Developments in Petroleum Science Vol. 29. Elsevier Science.

[22] Brooks, R.H. and Corey, A.T. (1964). Hydraulic properties of porous media, Hydrology Paper, Vol. 3, Colorado State University, Fort Collins.

[23] Preux, C., Malinouskaya, I., Nguyen, Q.L. and Tabary, R. (2018). Modeling and simulating multi-polymer injections. SPE Europec featured at 80th EAGE Conference and Exhibition, 11-14 June, Copenhagen, Denmark. DOI: https://doi.org/10.2118/190759-MS

[24] Archer J.S., Wall C.G. (1986). Petroleum engineering: principles and practice. London: Graham and Trotman.

[25] Craig, F. F. (1971) The Reservoir Engineering Aspects of Waterflooding. New York: H.L. Doherty Memorial Fund of AIME.

[26] Douarche, F., Da Veiga, S., Feraille, M., Enchéry, G., Touzani, S. and Barsalou, R. (2014). Sensitivity Analysis and Optimization of Surfactant-Polymer Flooding under Uncertainties. Oil & Gas Science and Technology Rev. IFP Energies nouvelles, 69(4) pp. 603-617. DOI: https://doi.org/10.2516/ogst/2013166

[27] PumaFlow^{TM} User Guide (2020).